J Mater Sci: Mater Electron
DOI 10.1007/s10854-017-8056-2

Lead(II) halide cinnamaldehyde thiosemicarbazone complexes as single source precursors for oleylamine-capped lead sulfide nanoparticles

Siphamandla C. Masikane[1] · Sixberth Mlowe[1] · Charles Gervas[1] · Neerish Revaprasadu[1] · Amol S. Pawar[2] · Shivram S. Garje[2]

Received: 5 July 2017 / Accepted: 14 October 2017

Abstract Different PbX_2 (X = AcO, Cl, Br, I) metal salts were complexed to cinnamaldehyde thiosemicarbazone ligand. The resulting complexes were characterised using Fourier Transform Infrared spectroscopy, ^{1}H and ^{13}C $\{^{1}H\}$ Nuclear Magnetic Resonance spectroscopy, elemental analysis and thermogravimetric analysis techniques. They were then used as single source precursors for the preparation of lead sulfide (PbS) nanoparticles using the colloidal thermolysis route where oleylamine is used as the passivating agent. Each SSP is thermolysed at reaction temperatures of 190, 230 and 270 °C. Predominantly cubic-shaped PbS nanoparticles were obtained, with an exception of the truncated nanocubes obtained from thermolysis of the SSP prepared from lead bromide. Varying particle sizes are obtained when the halogen is varied, ranging from ca. 50 to 400 nm. The optical absorbance of the PbS nanoparticles in the UV-Vis-NIR range was found to be blue-shifted when compared to bulk PbS.

1 Introduction

Lead sulfide (PbS) is a group IV–VI semiconducting material which has received unprecedented attention over the last decade, owing to its tunable electronic and morphological properties [1–3]. Regardless of its toxic nature [4], PbS has unique quantization effects, properties which are accompanied by a direct band gap of 0.41 eV at 300 K, and a large excitonic Bohr radius of 18 nm [5–7]. These interesting properties have captured the attention of researchers, who have explored many synthetic routes and applications of this material [8–10]. PbS in the nano-size regime also exhibits interesting physical and chemical properties. A good example is the tuning of its broad, near infrared band edge to the ultra violet range through the engineering of the particle size and morphology. This is an important feature for optoelectronic devices which allows the material to harness energy within this broad range [11]. For this purpose, PbS nanomaterials have potential applications in solar cells [12], NIR communications [11, 13], thermal and biological imaging [14], tuneable near infrared detectors [15] and light emitting diodes [16].

Synthesis protocols for PbS nanostructures, can utilize either multiple or single source precursors (SSPs) [6, 17–25]. Joo et al. [21], for example used lead chloride and sulfur dissolved in oleylamine as dual sources to synthesize PbS particles. The use of SSPs has recently been preferred for size and shape-control, due to high quality materials obtained previously [6, 22–25]. This is easily achieved through the decomposition or disintegration of the SSP, which is usually a metal–organic compound bearing the preformed metal–chalcogen bonds. Furthermore, the SSPs have the advantage of ascertained purity and stability under ambient conditions, as well as the omission of pre-reactions prior to nanomaterial-based fabrication processes. The majority of the work on lead complexes used as SSPs for PbS nanostructures has been dominated by thiolates such as dithiocarbamates, xanthates and thiosermicarbazides [6, 19, 25, 26]. Other

Electronic supplementary material The online version of this article (doi:10.1007/s10854-017-8056-2) contains supplementary material, which is available to authorized users.

✉ Neerish Revaprasadu
RevaprasaduN@unizulu.ac.za

[1] Department of Chemistry, University of Zululand, Private Bag X1001, Kwa-Dlangezwa 3886, South Africa

[2] Department of Chemistry, University of Mumbai, Vidyanagari, Santacruz (E), Mumbai 400 098, India

Published online: 19 October 2017

similar compounds continue to receive considerable attention mainly in other fields of research. For example, thiosemicarbazones which predominate in biological applications [27, 28]. Garje and co-workers have explored the use of these compounds as ligands for various metal complexes [29–33].

Although diverse fabrication protocols have been established for PbS nanomaterials [20, 23, 24, 34–37], very few allow easy access to size, shape and morphology control. As a result, solvent-based fabrication protocols such as the solvothermal method [38–40], address this issue by employing coordinating solvents which play a major role in: (i) lowering the decomposition temperature, and (ii) stabilizing nanomaterials during and after fabrication. Many coordinated solvents have been explored to achieve this, including non-toxic cetytrimethylammonium bromide (CTAB) and polyethylene glycol 400 (PEG-400) [38]. Long alkyl chain amines such as hexadecylamine and oleylamine, have taken precedence due to high efficiency in producing good quality nanostructures [41, 42].

Size and morphology control, in the context of SSPs, has mainly focused on organic ligands which can either be constituents within the SSPs or the capping agents [2, 43, 44]. Recent work has identified the addition of halogenated compounds to synthesis protocols as a means to control size, shape and phase of nanoparticles [45, 46]. Klinke et al. [46] investigated the morphology, size and phase of CdSe nanoparticles through the influence of the chemical structure and type of halogen atom introduced into the reaction. Very few reports have focused on inorganic ligands incorporated in the chemical structures of SSPs. To the best of our knowledge, these reports have been restricted to common anionic ligands such as Cl^-, CH_3COO^-, NO_3^-, SO_4^{2-}, PF_6^-, BPh_4^- and BF_4^- on Zn^{2+}, Ni^{2+}, Ce^{2+}, In^{3+}, Co^{2+}, Cu^+, Rh^0 and Cd^{2+} metal centres ([47], and references therein). However, studies that concentrate on the halogen series are rare, hence our recent report provided an opportunity towards this direction [48]. Our work demonstrated the size, shape and morphology control on CdS nanoparticles by altering the organic and halogen (Cl^- and Br^-) components of the Cd(II)-thiosemicarbazone complexes.

We have thus extended our work to further study the morphological evolution and possible effect on the properties of PbS nanoparticles, focusing on the broader halogen series (Cl^-, Br^- and I^-) complimented by a non-halogenated precursor. The nanoparticles are prepared by the solvothermal decomposition of halogenated and non-halogenated Pb(II)-cinnamaldehyde thiosemicarbazone complexes in oleylamine at different reaction temperatures.

2 Experimental details

2.1 Materials and methods

Tri-*n*-octylphosphine and oleylamine were purchased from Sigma-Aldrich. Acetone, methanol, cyclohexane and hexane were purchased from Merck. Lead(II) acetate trihydrate and lead(II) iodide were procured from S D Fine-Chem, while lead(II) chloride and lead(II) bromide were procured from Alfa-Aesar. All chemicals were used as received. The cinnamaldehyde thiosemicarbazone ligand and complexes were synthesized by previous methods [48, 49] with minor modifications detailed in the ESI.

Elemental analyses (C, H, N and S) of ligands and the corresponding Pb(II) complexes were carried out using a Thermo Finnigan Italy Model FLASH EA 1112 Series elemental analyser. The lead and chloride content was determined by the complexometric method and Volhard titration, respectively. Melting points of the ligand and the corresponding lead complexes were carried out on a Centrofix Scientific sales syndicate melting point apparatus. Infrared spectra of ligand and complexes were recorded on a Perkin Elmer Spectrum One FTIR Spectrometer and the measurements taken in the 4000–400 cm^{-1} range. Thermogravimetric analysis was carried out at 10 °C min^{-1} heating rate using a Perkin-Elmer Pyris 6 TGA from 30 to 700 °C in a closed perforated aluminium pan under N_2 gas. The ^1H and $^{13}C\{^1H\}$ NMR spectra were recorded on a Bruker-300 spectrophotometer, using DMSO-D_6 solvent. The chemical shifts are relative to internal standard, tetramethylsilane. Molar conductance measurements were made in dimethylformamide (DMF) (10^{-3} mol L^{-1}) using a Toshniwal conductivity meter.

Optical absorption measurements of the nanoparticles were carried out using a Perkin-Elmer Lambda 1050 NIR UV-Visible spectrophotometer. The samples were placed in silica cuvettes (1 cm path length), using hexane as a reference solvent. TEM and HRTEM analyses were performed using a JEOL 1400 TEM and JEOL 2100 HRTEM, respectively. Samples were prepared by placing a drop of dilute solution of nanoparticles on Formvar-coated grids (150 mesh) for TEM, and holey carbon grids for HRTEM. The samples were allowed to dry completely at room temperature and viewed at an accelerating voltage of 100 kV (TEM) and 200 kV (HRTEM), and images captured digitally using a Megaview III camera. The acquired images were further processed using Soft Imaging Systems iTEM software (TEM), and Gatan camera with Gatan software (HRTEM). A Zeiss Ultra Plus FEG SEM was used for surface morphology analysis, equipped with an Oxford detector EDX at 20 kV which uses Aztec software for elemental analysis. The samples were carbon coated using Quorum coater (Model Q150TE). Powder X-Ray Diffraction

(p-XRD) patterns were recorded in the high angle 2θ range of 20°–80° using a Bruker AXS D8 Advance X-Ray diffractometer, equipped with nickel filtered Cu Kα radiation (λ = 1.5406 Å) at 40 kV, 40 mA and at room temperature.

2.2 Synthesis of lead(II) cinnamaldehyde thiosemicarbazone (1)

In a round-bottom flask, was dissolved $Pb(OAc)_2{\cdot}3H_2O$ (966 mg, 2.54 mmol) in dry methanol (15.0 mL). To this colourless solution, was added a solution of cinnamaldehyde thiosemicarbazone (1.04 g, 5.09 mmol) in dry methanol (25.0 mL), under vigorous stirring. The resulting pale green-coloured mixture was continued to stir and refluxed for 10 h. The mixture was then cooled to room temperature, prior to evaporating the solvent under vacuum. The pale green solids were repeatedly washed with copious amounts of cyclohexane and *n*-hexane, in this order. The solids, which are the products, were dried under vacuum at room temperature. Yield: 1.16 g, 73.9%. M. P.: 136 °C. Elemental analyses for $PbC_{20}H_{20}N_6S_2$, % found (calcd): Pb: 33.90 (33.64). C: 39.32 (39.00). H: 3.14 (3.27). N: 13.38 (13.64). S: 10.18 (10.41). IR: 3480, 3355 cm^{-1} (υ_{NH2} asym. and sym.), 1556 cm^{-1} (υ_{C-N}), 973 cm^{-1} (υ_{C-S}), 503 cm^{-1} (υ_{Pb-N}); NMR (δ in ppm) ^{1}H: 6.89–8.05 (m, $NH_2 + C_6H_5$–CH=CH–CH=N), ^{13}C: 177.53 (C=S), 146.24 (CH=N), 138.00, 136.01 (CH=CH), 128.80, 128.59, 126.76, 125.65 (aromatic carbons).

2.3 Synthesis of lead(II) chloride cinnamaldehyde thiosemicarbazone (2)

In a round bottom flask, was prepared a solution of lead chloride (807 mg, 2.90 mmol) dissolved in deionised water (20.0 mL). To this solution, was added drop-wise a solution of cinnamaldehyde thiosemicarbazone (1.19 g, 5.80 mmol) in tetrahydrofuran (20.0 mL), under constant stirring. The reaction mixture was stirred for a further 24 h, at room temperature. A yellow-coloured precipitate was formed, filtered, washed with copious amounts of deionised water, and then finally dried under vacuum. Yield: 1.46 g, 73.0%. M.P.: 165 °C. Elemental analyses for $PbCl_2C_{20}H_{22}N_6S_2$ (%) found (calcd): Pb: 30.47 (30.08).C: 35.10 (34.88). H: 3.42 (3.21). N: 12.08 (12.20). S: 9.18 (9.31). Cl: 10.54 (10.29). IR: 3413 cm^{-1}, 3271 cm^{-1} (υ_{NH2} asymm. and symm.), 3161 cm^{-1} (υ_{N-H}), 1607 cm^{-1} (υ_{C-N}), 972 cm^{-1} (υ_{C-S}), 513 cm^{-1} (υ_{Pb-N}). NMR (δ in ppm) ^{1}H: 6.82–8.16 (m, $NH_2 + C_6H_5$–CH=CH–CH=N), 11.39 (s, NH), ^{13}C: 177.63 (C=S), 144.70 (CH=N), 138.83, 135.83 (CH=CH), 128.84, 128.80, 126.88, 125.03 (aromatic carbons).

2.4 Synthesis of lead (II) bromide cinnamaldehyde thiosemicarbazone $PbBr_2(cinnamtsczH)_2$ (3)

The reaction protocol used for **(2)** was followed. Cinnamaldehyde thiosemicarbazone (1.41 g, 6.84 mmol) and $PbBr_2$ (1.26 g, 3.42 mmol) were used. A yellow coloured precursor **(3)** was obtained. Yield: 2.19 g, 82.2%. M.P.: 172 °C. Elemental analyses for $PbBr_2C_{20}H_{22}N_6S_2$ (%) found (calcd): Pb: 26.79 (26.64), C: 30.97 (30.89), H: 2.64 (2.85), N: 10.67 (10.80), S: 8.08 (8.24). IR: 3422, 3276 cm^{-1} (υ_{NH2} asym. and sym.), 3165 cm^{-1} (υ_{N-H}), 1607 cm^{-1} (υ_{C-N}), 973 cm^{-1} (υ_{C-S}); 508 cm^{-1} (υ_{Pb-N}). NMR (δ in ppm) ^{1}H 6.82–8.17 (m, $NH_2 + C_6H_5$–CH=CH–CH=N), 11.39 (s, NH), ^{13}C: 177.61 (C=S), 144.71 (CH=N), 138.83, 135.82 (CH=CH), 128.84, 128.80, 126.88, 125.01 (aromatic carbons).

2.5 Synthesis of lead(II) iodide cinnamaldehyde thiosemicarbazone (4)

The reaction protocol used for **(2)** was followed. Cinnamaldehyde thiosemicarbazone (1.11 g, 5.40 mmol) and PbI_2 (1.25 g, 2.70 mmol) were used. A yellow coloured precursor (4) was obtained. Yield: 1.70 g, 72.0%. M.P.: 224 °C. Elemental analyses for $PbI_2C_{20}H_{22}N_6S_2$ (%) found (calcd): Pb: 23.25 (23.77).C: 27.94 (27.56). H: 2.24 (2.54). N: 9.32 (9.64). S: 7.12 (7.35). IR: 3419, 3287 cm^{-1} (υ_{NH2} asymm. and symm.), 3181 cm^{-1} (υ_{N-H}), 1579 cm^{-1} (υ_{C-N}), 978 cm^{-1} (υ_{C-S}), 499 cm^{-1} (υ_{Pb-N}). NMR (δ in ppm) ^{1}H: 6.82–8.16 (m, $NH_2 + C_6H_5$–CH=CH–CH=N), 11.39 (s, NH), ^{13}C: 177.60 (C=S), 144.69 (CH=N), 138.83, 135.83 (CH=CH), 128.85, 128.80, 126.88, 125.01 (aromatic carbons).

2.6 Preparation of lead sulfide nanoparticles

In a three-necked flask, equipped with a reflux condenser, thermometer and a rubber septum, was charged oleylamine (3.00 g) which was subsequently heated and maintained to an appropriate temperature (190, 230 or 270 °C). To the heated oleylamine, was injected a suspension of a complex (250 mg) dispersed in tri-*n*-octylphosphine (6.0 mL), using a glass syringe. The reaction is cooled to room temperature after 2 h. The solids were separated by precipitation using methanol, followed by centrifugation. The resultant precipitate was then washed three-times using acetone; the supernatant was discarded. The samples were dissolved in hexane, prior to spectroscopic and TEM analyses. Acetone was used as a dispersing solvent for HRTEM analyses.

3 Results and discussion

The study investigates the influence of halogen ligands on the decomposition behaviour of the Pb(II)-cinnamaldehyde

thiosemicarbazone complexes, which is subsequently monitored through size and morphology of PbS nanoparticles produced. Complementary to this, the complexes were prepared from the PbX_2 (X = Cl, Br and I) series, as illustrated in Scheme 1a. The preparation protocols are adapted from the procedures which previously afforded Cd(II) counterparts [48], where the 1:2 (ligand to metal salt) is essential to form structurally-stable compounds. The hydrated lead acetate salt, $Pb(OAc)_2{\cdot}3H_2O$, was used to prepare a non-halogenated complex which would serve as a reference material, Scheme 1b. The structures of the complexes (ESI, Fig. S1) were elucidated through use of FT-IR and ^1H and $^{13}C\{^1H\}$ NMR spectroscopic data acquired from the complexes (ESI, Figs. S2–S18).

A prominent band appearing at around 1625 cm^{-1} is typical of the azomethine (C=N) functional group [50, 51]. This is indicative of a successful condensation between the aldehyde and amino moieties, thus forming the desired cinnamaldehyde thiosemicarbazone ligand (Scheme 1). When the ligand is complexed to Pb salts, the υ(C=N) band shifts to lower wave numbers by 10–15 cm^{-1}, this suggests that the nitrogen atom of the azomethine group has bonded to the Pb atom [52–54]. A similar trend is observed for the secondary amine functional group which appears at 3156 cm^{-1} in the ligand. Interestingly, this υ(NH) band is absent in non-halogenated-**(1)** complex which thus prompts deprotonation. Due to this observation, accompanied by the absence of the acetate component in non-halogenated-**(1)** complex, we propose that an acetic acid by-product is formed (Figs. S2 and S3). A plausible mechanism is illustrated in Scheme 2.

The results from the elemental analysis and molar conductance studies on the complexes corroborated with the spectroscopic data. The complexes were found to be relatively pure, and the anticipated 1:2 metal to ligand stoichiometry was confirmed, as suggested by the elemental analysis data. Molar conductance readings were taken from the pre-made 10^{-3} M solutions of complexes in dimethylformamide, and were recorded to be 13.5, 25.4, 19.5, and 14.8 Ω^{-1} cm^2 mol^{-1} for complexes **(1), (2), (3)** and **(4)**, respectively. These molar conductance readings are consistent with ionic adducts or uncharged complexes, i.e. non-electrolyte properties [55].

The halogen ligands have been found to exert an influence on the thermal stability of the complexes, although no significant trend is observed (Fig. 1a). The chlorido-**(2)** and iodido-**(4)** complexes show two relatively clean decomposition patterns, whereas those of the remaining complexes are undefined. Nonetheless, the solid residues retained from this thermogravimetric analysis study were matched to the PbS (card number: 00-005-0592) as shown in Fig. 1b.

The morphological properties of the lead sulfide (PbS) nanoparticles, are influenced by both the thermolytic reaction temperature and the type of halogen ligand incorporated within the lead complexes. The investigated halogen series consist of chloride (Cl), bromide (Br) and iodide (I)-incorporated SSPs, where the precursor obtained from lead acetate serves as a reference material. Prior to this investigation, it was necessary to confirm whether PbS nanoparticles had formed after thermolytic processes. For this purpose, p-XRD and scanning electron microscopy energy dispersive X-ray (SEM-EDX) studies were conducted.

The p-XRD patterns confirmed that the products of the thermolytic reactions correspond to PbS (Fig. 2). The patterns also reveal the formation of face centered cubic (FCC)

Scheme 1 The synthesis of **a** $[PbX_2(LH)_2]$, and **b** $[PbL_2]$ precursors

(a)

$$PbX_2 + 2(LH) \xrightarrow[\text{R.T., 24 h}]{H_2O/THF} PbX_2(LH)_2$$

(b)

$$Pb(OAc)_2{\cdot}3H_2O + 2(LH) \xrightarrow[\text{Reflux, 10 h}]{MeOH} PbL_2 + CH_3COOH$$

LH =

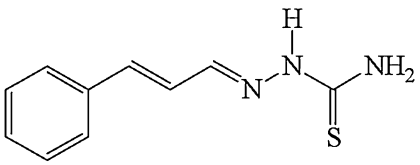

L =

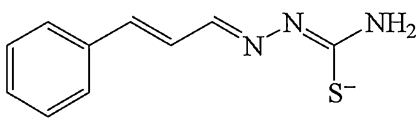

Scheme 2 Mechanism illustrating the formation of a non-halogenated-**(1)** complex

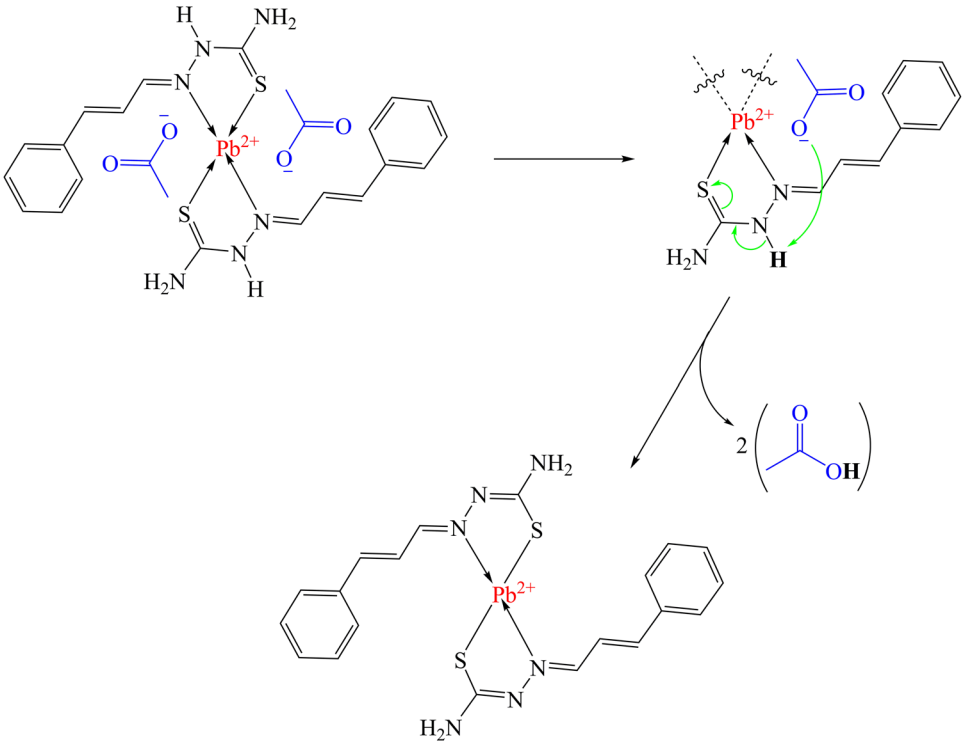

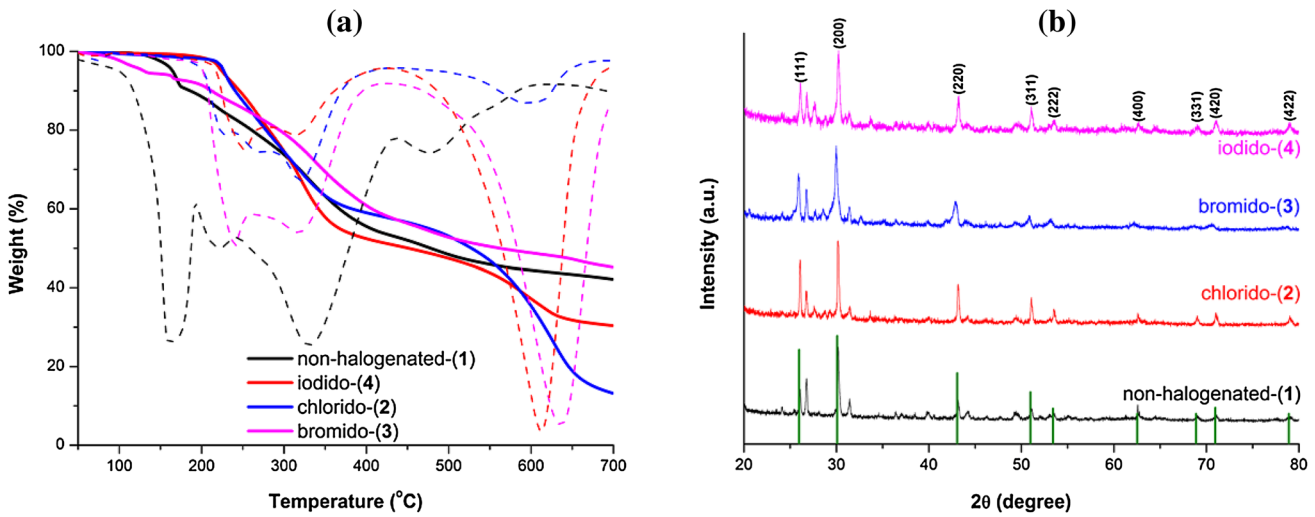

Fig. 1 **a** Thermogravimetric (solid line) and differential thermogravimetric (dash line) decomposition profiles of the complexes, with the corresponding **b** powder X-ray diffraction patterns of the residues obtained

rock-salt structure (card number: 00-005-0592) of PbS. This was observed for the PbS nanoparticles obtained from all the precursors, there was no phase change observed when temperature was varied. The additional unindexed peaks observed in the diffraction patterns on Fig. 1b compared to those of Fig. 2, can be attributed to impurities resulting from high decomposition temperatures in the absence of a capping agent. This clearly demonstrates the advantages and/or capabilities of a capping agent in lowering the decomposition energy of the precursor to afford phase-pure nanomaterials. The SEM-EDX studies also confirmed the material to have Pb and S components (Figs. S17–S20). Interestingly, substantial amounts of halogen content were detected in some of the samples. Due to the nature of our study, no further investigations were conducted to determine in what chemical form the halogen species exist in/within the material. However, the elemental mapping images suggest homogeneity throughout the samples (Fig. 3). This could indicate either

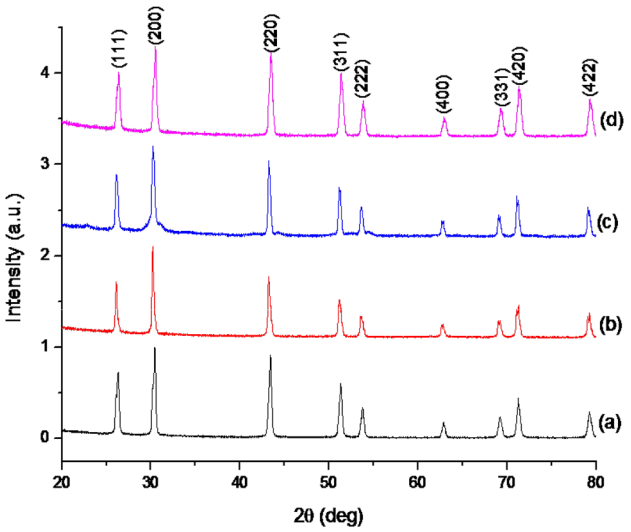

Fig. 2 Powder X-ray diffraction (XRD) patterns of PbS nanoparticles synthesized at 270 °C using lead thiosemicarbazone complexes made from (*a*) lead acetate (*b*) lead chloride (*c*) lead bromide and (*d*) lead iodide metal salts

halogen-PbS solid solution, or adhesion by the halogens on the PbS surfaces similarly to inorganic capping groups reported elsewhere [56–58].

From the TEM studies, it was evident that the size of the nanoparticles increases with reaction temperature from 190 to 270 °C. This is generally attributed to the Ostwald ripening growth process. At relatively lower reaction temperature (190 °C), close to uniform particle sizes are obtained from the halogenated complexes **(2), (3)** and **(4)** (Figs. 4a, 5a, c) respectively. An increase to 230 °C adversely affects the monodispersity, for example, the nanoparticles obtained from chlorido-**(2)** exhibits a mixture of three average sizes where the largest particles are ± 100 nm (Fig. 4b). A similar trend was observed for the bromido-**(3)** and iodido-**(4)** complexes (ESI Fig. S21c and e, respectively). A further increase to 270 °C showed an interesting observation, the largest particle sizes obtained from chlorido-**(2)**, bromido-**(3)** and iodido-**(4)** are found to be ± 100, ± 200 and ± 400 nm, respectively. Coincidently, this observation coincides with an increasing trend in atomic diameter of elements in the group VII halogen series. Furthermore, improvement in monodispersity drops significantly down the halogen series. At this point, there is insufficient evidence to conclude if this observation is as a result of either electronic or steric differences exerted by the halogens on the decomposition of the complex.

The non-halogenated-**(1)** complex, on the other hand, exhibits different behaviour to that of the halogen derivatives. The nanoparticles agglomerate at lower-to-moderate reaction temperatures, 190 and 230 °C, thus making it difficult to investigate and conclude on the sizes of the as-prepared nanoparticles (Fig. S21a and b, respectively). However, as the temperature is raised to 270 °C, pronounced and almost uniform cubic-shaped nanoparticles are obtained (Fig. 6a).

Although the study has failed to achieve a uniform and controlled size of the nanoparticles, the opposite was observed with regards to their shape. The work by Cao et al. [38] has established a detailed growth mechanism for PbS nanoparticles. Briefly, the mechanism involves the nucleation where growth starts from the rock salt like seed crystal of PbS. These seed crystals are responsible for the final morphology of the material obtained. It is known that the PbS seeds are tetradecahedrons, i.e. truncated cubes with exposing [100] and [111] facets. The growth along <100> facet would lead to pods, whereas, preferential growth

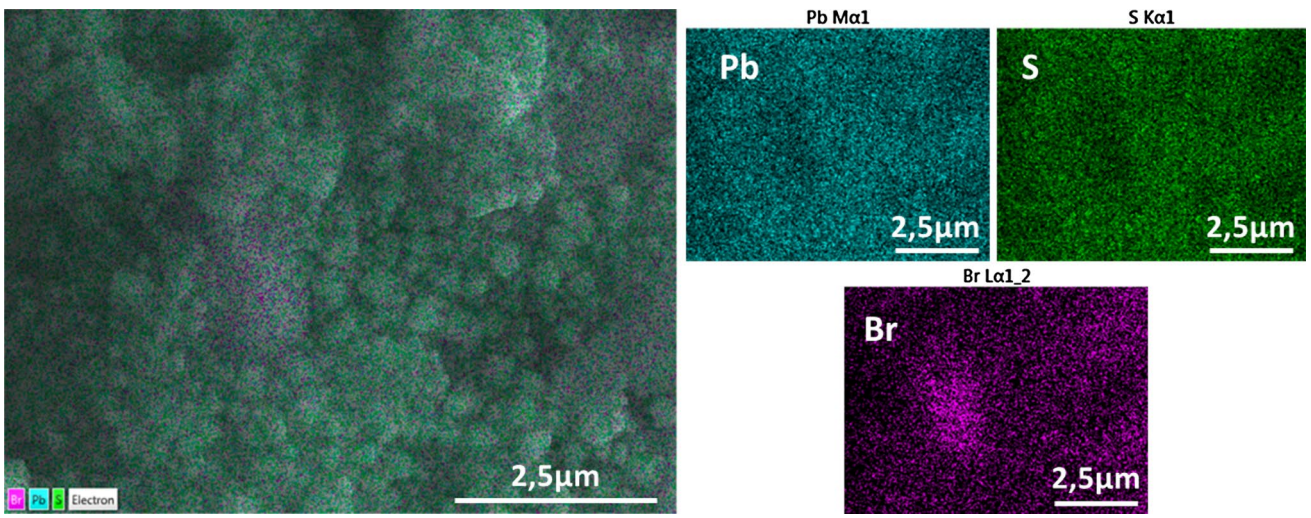

Fig. 3 Representative elemental mapping images for PbS nanoparticles obtained from bromido-**(3)** at 270 °C

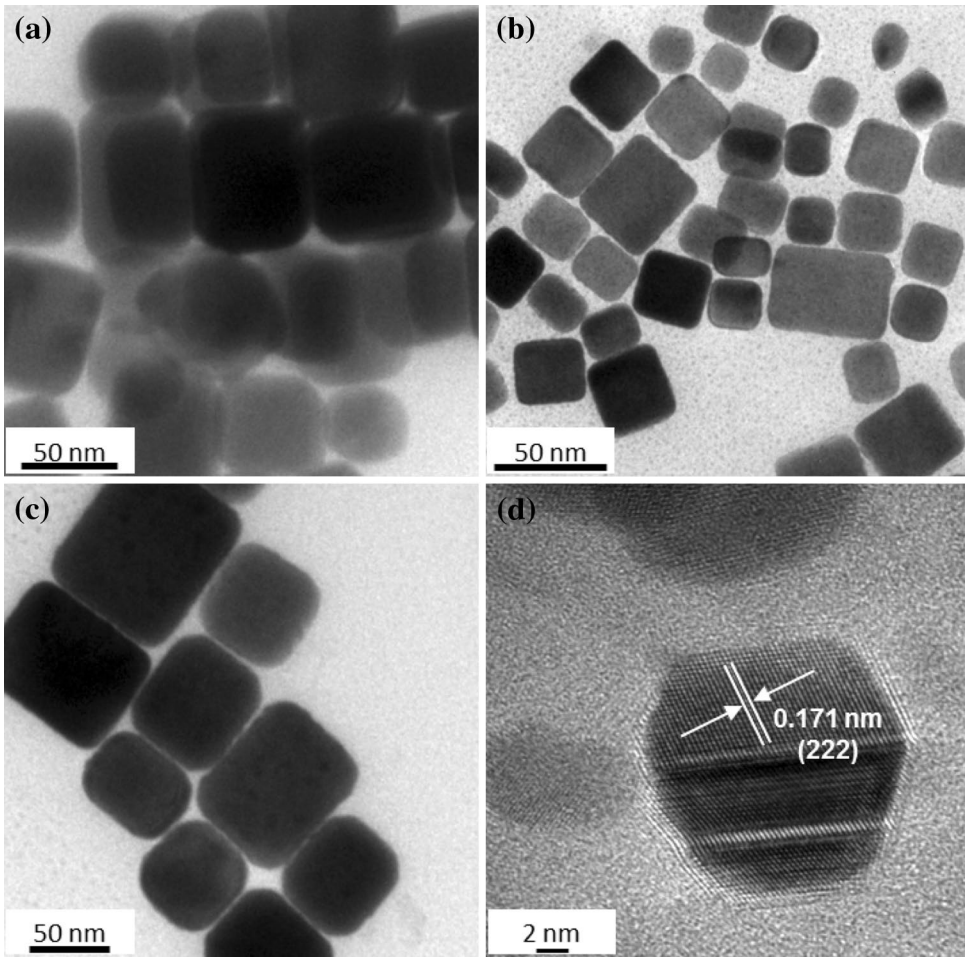

Fig. 4 TEM images of PbS nanoparticles obtained from the thermolysis of chlorido-**(2)** complex in oleylamine at **a** 190 °C, **b** 230 °C, **c** 270 °C, as well as **d** the HRTEM image obtained at 230 °C decomposition temperature

along <111> direction would lead to cubes. Therefore, the final shape of the PbS nanoparticles will depend on relative growth along <100> and <111> directions. Crystallographic [111] facets of the rock salt structure have high intrinsic surface energy. This leads to higher growth rate along <111> direction resulting into cubes. Thus, stabilizing surfactants which can block or enhance growth of certain facet, temperature and concentration of precursor are among reaction parameters used to manipulate the morphology of the materials prepared. Certain stabilizing agents like amines are known to stabilise [100] facets, thus indirectly enhancing growth along <111> direction. This leads to growth of octopods along <111> direction, the further repining, i.e. space filling between octopods results into final cubes. In our work, we have observed the role of the halogen ligands incorporated within the precursor complexes, in addition to reaction temperature, to have had an influence on the morphology of the nanoparticles. Interestingly, the shape of the nanoparticles become more pronounced as the reaction temperature increases, when the non-halogenated-**(1)** complex and chlorido-**(2)** complex are used. However, the opposite is observed for the bromido-**(3)** and iodido-**(4)** complexes. Additionally, the nanoparticles obtained from the bromido-**(3)** complex exhibit truncated cubic-like shape at a relatively lower temperature (190 °C), which is different from the cubes observed at other temperatures across all complexes (Fig. 5a). The clearly visible lattice fringes observed from the HRTEM image confirmed that the nanoparticles are crystalline, regardless of the morphology (Figs. 6b and S22). It was further noted that nanoparticles obtained from the chlorido-**(2)** and iodido-**(4)** complexes were disintegrating into smaller nanoparticles, while acquiring lattice fringes (Figs. 4d, 5d) respectively. The absence of the chloride content in the nanoparticles obtained from chlorido-**(2)** ruled out the possibility of the role of halogens in such a phenomenon.

As a result of the relatively varied morphology of PbS nanoparticles obtained from bromido-**(3)**, further studies were carried out. For this purpose, UV-Vis-NIR optical absorption studies were conducted. As shown in ESI Fig. S23, these NPs absorb strongly in Visible-NIR region due to their strong size quantization [59]. Remarkably, the influence of temperature gave a strong absorption band 715 nm (1.73 eV) from truncated cube-shaped NPs synthesized at

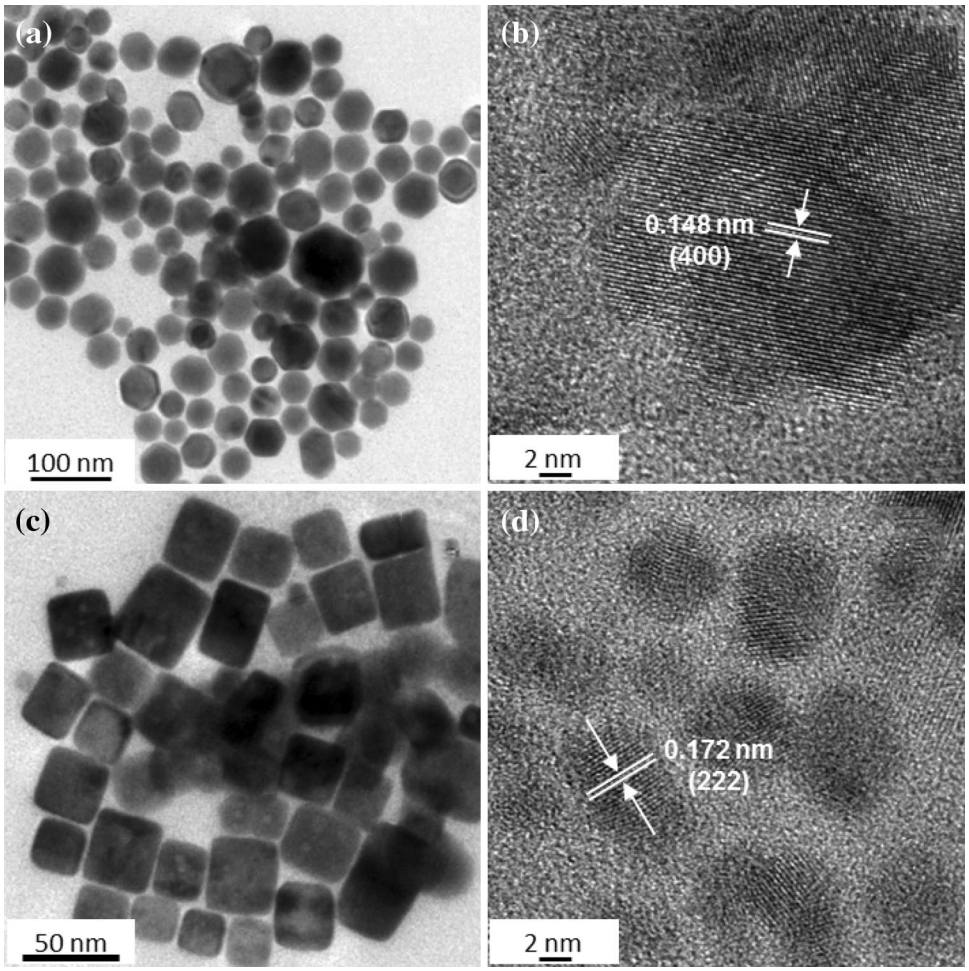

Fig. 5 TEM images of PbS nanoparticles obtained from the thermolysis of **a** bromido-**(3)** at 190 °C, and **c** iodido-**(4)** at 190 °C, with the corresponding HRTEM images obtained at **b** 190 °C and **d** 270 °C decomposition temperatures, respectively

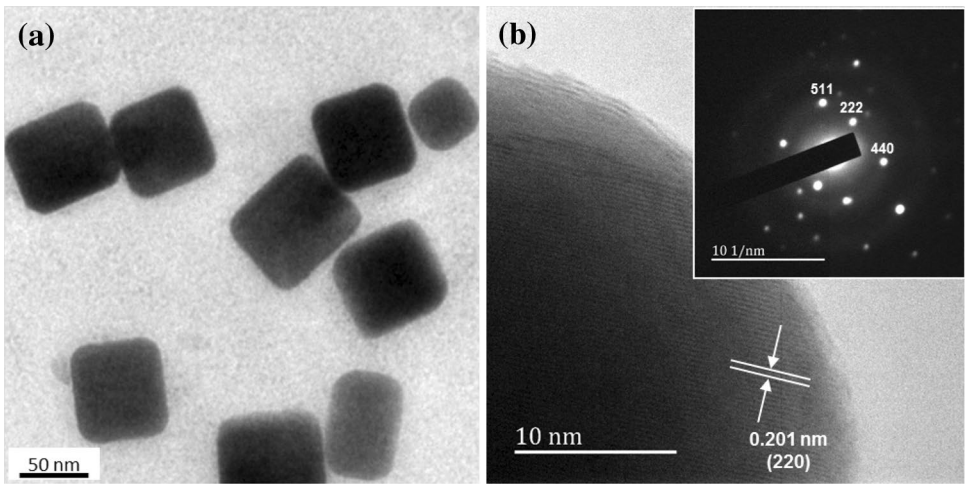

Fig. 6 The **a** TEM image of PbS nanoparticles obtained from the thermolysis of non-halogenated-**(1)** at 270 °C, and the corresponding **b** HRTEM image (insert: FFT of PbS nanoparticles)

190 °C. At relatively higher reaction temperatures, 230 and 270 °C, the samples exhibited strong absorption peaks at much lower wavelength 395 nm (3.14 eV), progressively blue shifted from both the bulk material and nanoparticles obtained at 190 °C. The absorption spectra wavelength for the 190 °C sample is consistent with literature reports, however, a decrease in absorption wavelength (blue shift) at higher reaction temperatures is not commonly reported.

We then further conducted absorption measurements of NPs obtained from other complexes. As a result of the interesting observation made from bromido-**(3)** at higher temperatures, we focused our absorption studies on NPs

synthesized at 270 °C (Fig. 7). The PbS NPs obtained from the iodido-**(4)** complex showed a broad absorption in the NIR region around 1150 nm (1.08 eV) and an excitonic absorption peak at 390 nm (3.18 eV). The nanoparticles obtained from the non-halogenated-**(1)** and chlorido-**(2)** complexes showed absorption bands around 500 nm (2.48 eV) and 1100 nm (1.13 eV), respectively. The bromido-**(3)** complex showed an excitonic absorption peak at around 390 nm (3.18 eV). The absorption band energies observed here are typical of PbS nanoparticles [60]. The differences in band-edge excitonic features could be due to the structural differences in the single source precursors.

4 Conclusions

In this study, PbX_2 (X = Cl, Br, I) and non-halogenated Pb^{2+} cinnamaldehyde thiosemicarbazone complexes have been prepared in good yields and characterized fully by elemental analysis, FT-IR and ^{1}H and ^{13}C $\{^{1}H\}$ NMR spectroscopy techniques. The thermogravimetric analysis confirmed that the complexes are suitable for use as single source molecular precursors (SSPs) towards the synthesis of PbS, albeit at moderate decomposition temperatures. Thus, the SSPs were used to demonstrate the role of the halide ligands on the size and shape of the PbS nanoparticles, as well as their optical absorption properties. The formation of PbS material (card number: 00-005-0592) through the oleylamine-mediated hot-injection reaction was confirmed using powder X-ray diffraction and energy dispersive X-ray (EDX) spectroscopy. Significant amounts of the bromide and iodide elements were detected in nanoparticles obtained from the corresponding complexes. Average particle sizes are found to be in the 50–400 nm range, were estimated using transmission electron microscopy imaging; increase in reaction temperature results in an increase in particle size. Furthermore, the dominant cubic-shape morphology becomes less pronounced down the halogen series. Interestingly, the bromide-incorporated complex produced truncated cube-shaped nanoparticles at relatively lower temperatures. The optical absorbance for all nanoparticles were found to be blue-shifted when compared to the bulk material; band gaps of between 1.08 to 3.18 eV were obtained.

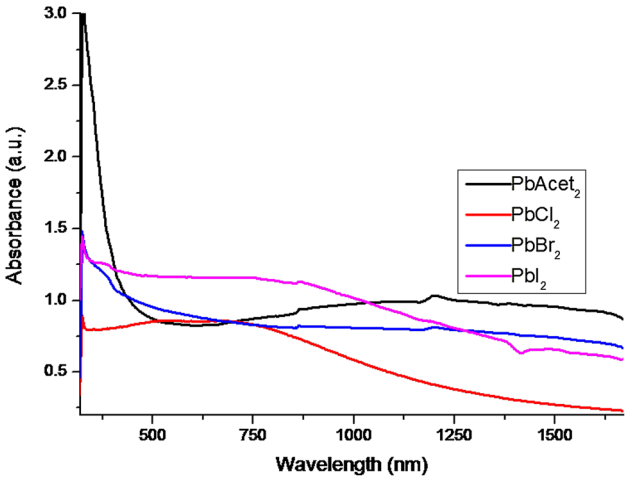

Fig. 7 The UV-Vis-NIR absorption spectra of oleylamine-capped PbS nanoparticles synthesized at 270 °C

Acknowledgements The authors are grateful to the National Research Foundation (NRF), South Africa (NRF Grant Number 64820), the India–Brazil–South Africa (IBSA) program, Royal Society Department For International Development (RS-DFID) program and the Department of Science and Technology (DST)-PURSE, India, for financial support.

References

1. M. Salavati-Niasari, A. Sobhani, F. Davar, J. Alloys Compd. **507**, 77 (2010)
2. N. Reilly, M. Wehrung, R. Andrew, O. Dell, L. Sun, Mater. Chem. Phys. **147**, 1 (2014)
3. K.T. Yong, Y. Sahoo, K.R. Choudhury, M.T. Swihart, J.R. Minter, P.N. Prasad, Chem. Mater. **18**, 5965 (2006)
4. J.T. Zelikoff, J.H. Li, A. Hartwig, X.W. Wang, M. Costa, T.G. Rossman, Carcinogenesis **9**, 1727 (1988)
5. I. Chakraborty, S.P. Moulik, J. Nanoparticle Res. **7**, 237 (2005)
6. L.D. Nyamen, V.S.R. Rajasekhar Pullabhotla, A.A. Nejo, P.T. Ndifon, J.H. Warner, N. Revaprasadu, Dalton Trans. **41**, 8297 (2012)
7. H. Karami, M. Ghasemi, S. Matini, Int. J. Electrochem. Sci. **8**, 11661 (2013)
8. K. Ramasamy, M.A. Malik, N. Revaprasadu, P. O'Brien, Chem. Mater. **25**, 3551 (2013)
9. K.C. Preetha, T.L. Remadevi, Mater. Sci. Semicond. Process. **16**, 605 (2013)
10. M. Corricelli, D. Altamura, L. De Caro, A. Guagliardi, A. Falqui, A. Genovese, A. Agostiano, C. Giannini, M. Striccoli, M.L. Curri, Cryst. Eng. Comm. **13**, 3988 (2011)
11. K.N. Bourdakos, D.M.N.M. Dissanayake, T. Lutz, S.R.P. Silva, R.J. Curry, Appl. Phys. Lett. **92**, 2008 (2008)
12. S. Günes, K.P. Fritz, H. Neugebauer, N.S. Sariciftci, S. Kumar, G.D. Scholes, Sol. Energy Mater. Sol. Cells **91**, 420 (2007)
13. F.C.J.M. Van Veggel, Chem. Mater. **26**, 111 (2014)
14. J.D. Patel, Mater. Sci. Appl. **03**, 125 (2012)
15. M. Asad, M. Fathipour, M.H. Sheikhi, M. Pourfath, Sens. Actuators A **220**, 213 (2014)
16. L. Sun, J.J. Choi, D. Stachnik, A.C. Bartnik, B.-R. Hyun, G.G. Malliaras, T. Hanrath, F.W. Wise, Nat. Nanotechnol. **7**, 369 (2012)
17. A.O. Nejo, A.A. Nejo, R.V.S.R. Pullabhotla, N. Revaprasadu, J. Alloys Compd. **537**, 19 (2012)
18. C. Gervas, S. Mlowe, M.P. Akerman, I. Ezekiel, T. Moyo, N. Revaprasadu, Polyhedron **122**, 16 (2017)
19. S. Ye, Y. Ye, Y. Ni, Z. Wu, J. Cryst. Growth **284**, 172 (2005)
20. T. Trindade, P. O'Brien, X. Zhang, M. Motevalli, J. Mater. Chem. **7**, 1011 (1997)
21. J. Joo, H.B. Na, T.Y. Yu, J.H. Yu, Y.W. Kim, F. Wu, J.Z. Zhang, T. Hyeon, J. Am. Chem. Soc. **125**, 11100 (2003)
22. G.B. Shombe, E.B. Mubofu, S. Mlowe, N. Revaprasadu, Mater. Lett. **185**, 17 (2016)

23. D. Berhanu, K. Govender, D. Smyth-Boyle, M. Archbold, D.P. Halliday, P. O'Brien, Chem. Commun. (2016). doi:10.1039/B612934J
24. I. Jen-La Plante, T.W. Zeid, P. Yang, T. Mokari, J. Mater. Chem. **20**, 6612 (2010)
25. N.O. Boadi, M.A. Malik, P. O'Brien, J.A.M. Awudza, Dalton Trans. **41**, 10497 (2012)
26. M.A. Malik, M. Afzaal, P. O'Brien, Chem. Rev. **110**, 4417 (2010)
27. S. Bhakat, A. Chakraborty, S.P. Dash, A.K. Panda, R. Acharyya, A. Biswas, S. Mukhopadhyay, S. Bhutia, A. Crochet, Y.P. Patil, M. Nethaji, R. Dinda, Dalton Trans. **44**, 6140 (2015)
28. E. Pahontu, F. Julea, T. Rosu, V. Purcarea, Y. Chumakov, P. Petrenco, A. Gulea, J. Cell. Mol. Med. **19**, 865 (2015)
29. B.P. Bade, S.S. Garje, Y.S. Niwate, M. Afzaal, P. O'Brien, Chem. Vap. Depos. **14**, 292 (2008)
30. S.D. Disale, S.S. Garje, Appl. Organometal. Chem. **24**, 734 (2010)
31. J.B. Biswal, S.S. Garje, Synth. React. Inorg. Met.-Org. Nano-Met. Chem. **43**, 461 (2013)
32. A.S. Pawar, S.S. Garje, Bull. Mater. Sci. **38**, 1843 (2015)
33. A.S. Pawar, S. Mlowe, S.S. Garje, M.P. Akerman, N. Revaprasadu, Inorg. Chim. Acta **463**, 7 (2017)
34. S. Axnanda, M. Scheele, E. Crumlin, B.H. Mao, R. Chang, S. Rani, M. Faiz, S.D. Wang, A.P. Alivisatos, Z. Liu, Nano Lett. **13**, 6176 (2013)
35. Y. Zhao, X.H. Liao, J.M. Hong, J.J. Zhu, Mater. Chem. Phys. **87**, 149 (2004)
36. M.R. Karim, M.D. Aktaruzzaman, M. Ashrafuzzaman, M.D.B. Zaman, Chalcogenide Lett. **11**, 531 (2014)
37. M. Behboudnia, M. Behboudnia, A. Habibi-Yangjeh, A. Khodayari, A. Khodayari, Y. Jafari-Tarzanag, Bull. Korean Chem. Soc. **29**, 53 (2008)
38. Y. Cao, P. Hu, D. Jia, Nanoscale Res. Lett. **7**, 668 (2012)
39. N. Wang, X. Cao, L. Guo, S. Yang, Z. Wu, ACS Nano **2**, 184 (2008)
40. Y. Ji, D. Yang, H. Zhang, X. Ma, J. Xu, D. Que, Solid State Phenom. **197**, 99–100 (2004)
41. M. Green, J. Mater. Chem. **20**, 5797 (2010)
42. Y. Yin, A.P. Alivisatos, Nature **437**, 664 (2005)
43. P.S. Nair, G.D. Scholes, J. Mater. Chem. **16**, 467 (2006)
44. M.S. Bakshi, Cryst. Growth Des. **16**, 1104 (2016)
45. J. Zhang, J. Gao, E.M. Miller, J.M. Luther, M.C. Beard, ACS Nano **8**, 614 (2014)
46. F. Gerdes, C. Navío, B.H. Juárez, C. Klinke, Nano Lett. **17**, 4165 (2017)
47. R. Gaur, P. Jeevanandam, New J. Chem. **39**, 9442 (2015)
48. A.S. Pawar, S.C. Masikane, S. Mlowe, S.S. Garje, N. Revaprasadu, Eur. J. Inorg. Chem. **2016**, 366 (2016)
49. F.E. Anderson, C.J. Duca, J.V. Scudi, J. Am. Chem. Soc. **73**, 4967 (1951)
50. C.H. Collins, A.M. Lyne, J.M. Grange, *Microbiological Methods*, 6th edn. (Butterworths, Oxford, 1989)
51. M.A. Ali, S.E. Livingstone, D.J. Philips, Inorg. Chim. Acta **7**, 179 (1973)
52. A. Saxena, J.K. Koacher, J.P. Tandon, Inorg. Nucl. Chem. Lett. **17**, 229 (1981)
53. A. Saxena, J.P. Tandon, K.C. Molloy, J.J. Zuckerman, Inorg.Chim. Acta **63**, 71 (1982)
54. A.K. Varshney, S. Varshney, H.L. Singh, Bull. Pol. Acad. Sci. Chem. **45**, 373 (1997)
55. W.J. Geary, Coord. Chem. Rev. **7**, 81 (1971)
56. M. Saruyama, M. Kanehara, T. Teranishi, J. Am. Chem. Soc. **132**, 3280 (2010)
57. M. Meyns, F. Iacono, C. Palentia, J. Geweke, M.D. Coderch, U.E.A. Fitt-schen, J.M. Gallego, R. Otero, B.H. Juárez, C. Klinke, Chem. Mater. **26**, 1813 (2014)
58. J. Tang, K.W. Kemp, S. Hoogland, K.S. Jeong, H. Liu, L. Levina, M. Fu-rukawa, X. Wang, R. Debnath, D. Cha, K.W. Chou, A. Fischer, A. Amassian, J.B. Asbury, E.H. Sargent, Nat. Mater. **10**, 765 (2011)
59. Y. Wang, A. Suna, W. Mahler, R. Kasowski, J. Chem. Phys. **87**, 7315 (1987)
60. F. Jähnig, D. Bozyigit, O. Yarema, V. Wood, APL Mater. **3**,01 (2015)